Resonant-enhanced full-color emission of quantum-dot-based micro LED display technology

Hau-Vei Han,[1] Huang-Yu Lin,[1] Chien-Chung Lin,[2,5] Wing-Cheung Chong,[3] Jie-Ru Li,[1] Kuo-Ju Chen,[1] Peichen Yu,[1] Teng-Ming Chen,[4] Huang-Ming Chen,[1] Kei-May Lau,[3] and Hao-Chung Kuo[1,6]

[1]*Department of Photonics and Institute of Electro-Optical Engineering, National Chiao Tung University, Hsinchu 30010, Taiwan*
[2]*Institute of Photonic System, National Chiao Tung University, Tainan 711, Taiwan*
[3]*Department of Electric and Computer Engineering, Hong Kong University of Science and Technology, Kowloon 999077, Hong Kong, China*
[4]*Phosphors Research Laboratory, Department of Applied Chemistry, National Chiao Tung University, Hsinchu 30010, Taiwan*
[5]*chienchunglin@faculty.nctu.edu.tw*
[6]*hckuo@faculty.nctu.edu.tw*

Abstract: Colloidal quantum dots which can emit red, green, and blue colors are incorporated with a micro-LED array to demonstrate a feasible choice for future display technology. The pitch of the micro-LED array is 40µm, which is sufficient for high-resolution screen applications. The method that was used to spray the quantum dots in such tight space is called Aerosol Jet technology which uses atomizer and gas flow control to obtain uniform and controlled narrow spots. The ultra-violet LEDs are used in the array to excite the red, green and blue quantum dots on the top surface. To increase the utilization of the UV photons, a layer of distributed Bragg reflector was laid down on the device to reflect most of the leaked UV photons back to the quantum dot layers. With this mechanism, the enhanced luminous flux is 194% (blue), 173% (green) and 183% (red) more than that of the samples without the reflector. The luminous efficacy of radiation (LER) was measured under various currents and a value of 165 lm/Watt was recorded.

References and links

1. E. F. Schubert and J. K. Kim, "Solid-State Light Sources Getting Smart," Science **308**(5726), 1274–1278 (2005).
2. S. Pimputkar, J. S. Speck, S. P. DenBaars, and S. Nakamura, "Prospects for LED lighting," Nat. Photonics **3**(4), 180–182 (2009).
3. K.-J. Chen, H.-V. Han, H.-C. Chen, C.-C. Lin, S.-H. Chien, C.-C. Huang, T.-M. Chen, M.-H. Shih, and H.-C. Kuo, "White Light Emitting Diodes with Enhanced CCT Uniformity and Luminous Flux Using ZrO2 Nanoparticles," Nanoscale **6**(10), 5378–5383 (2014).
4. P. Waltereit, O. Brandt, A. Trampert, H. T. Grahn, J. Menniger, M. Ramsteiner, M. Reiche, and K. H. Ploog, "Nitride semiconductors free of electrostatic fields for efficient white light-emitting diodes," Nature **406**(6798), 865–868 (2000).
5. J. K. Park, C. H. Kim, S. H. Park, H. D. Park, and S. Y. Choi, "Application of strontium silicate yellow phosphor for white light-emitting diodes," Appl. Phys. Lett. **84**(10), 1647–1649 (2004).
6. T.-F. Wu, Y.-C. Wu, and Z.-Y. Su, "Design considerations for single-stage electronic ballast with dimming feature," IEEE Transactions on Industry Applications, **37**(5), 1537–1543 (2001).
7. P. Yeh and C. Gu, *Proceedings of liquid crystal displays* (John Wiley & Sons, 123, 2010).
8. H.-P. Shieh, Y.-P. Huang, M.-J. Su, and S.-T. Wu, "Single cell-gap transflective color TFT-LCD by using image-enhanced reflector," *Proceedings of the Sixth Chinese Symposium on Optoelectronics* (IEEE, 2003), pp. 270–272.

9. C.-C. Chen, C.-Y. Wu, and T.-F. Wu, "LED back-light driving system for LCD panels," in *Applied Power Electronics Conference and Exposition, 2006. APEC'06. Twenty-First Annual IEEE Conference* (IEEE, 2006), pp 381.
10. S. Riehemann, C. Grossmann, U. Vogel, B. Richter, R. Herold, and G. Notni, "Ultra small OLED pico projector," Optik Photonik **4**(2), 34–36 (2009).
11. Z. L. Liu, W. C. Chong, K. M. Wong, K. H. Tam, and K. M. Lau, "A Novel BLU-Free Full-Color LED Projector using LED on Silicon Micro-Displays," IEEE Photonics Technol. Lett. **25**(23), 2267–2270 (2013).
12. Z. J. Liu, W. C. Chong, K. M. Wong, and K. M. Lau, "360 PPI flip-chip mounted active matrix addressable light emitting diode on silicon (LEDoS) micro-displays," J. Displ. Technol. **9**(8), 678–682 (2013).
13. Z. J. Liu, W. C. Chong, K. M. Wong, C. W. Keung, and K. M. Lau, "Investigation of Forward Voltage Uniformity in Monolithic Light-Emitting Diode Arrays," IEEE Photonics Technol. Lett. **25**(13), 1290–1293 (2013).
14. Z. Gong, E. Gu, S. R. Jin, D. Massoubre, B. Guilhabert, H. X. Zhang, M. D. Dawson, V. Poher, G. T. Kennedy, P. M. W. French, and M. A. A. Neil, "Efficient flip-chip InGaN micro-pixellated light-emitting diode arrays: Promising candidates for micro-displays and colour conversion," J. Phys. D Appl. Phys. **41**(9), 094002 (2008).
15. M. A. Hines and P. Guyot-Sionnest, "Synthesis and Characterization of Strongly Luminescing ZnS-Capped CdSe Nanocrystals," J. Phys. Chem. **100**(2), 468–471 (1996).
16. H. Mattoussi, J. M. Mauro, E. R. Goldman, G. P. Anderson, V. C. Sundar, F. V. Mikulec, and M. G. Bawendi, "Self-assembly of CdSe-ZnS quantum dot bioconjugates using an engineered recombinant protein," J. Am. Chem. Soc. **122**(49), 12142–12150 (2000).
17. B. Dabbousi, J. Rodriguez-Viejo, F. V. Mikulec, J. Heine, H. Mattoussi, R. Ober, K. Jensen, and M. Bawendi, "(CdSe) ZnS core-shell quantum dots: synthesis and characterization of a size series of highly luminescent nanocrystallites," J. Phys. Chem. B **101**(46), 9463–9475 (1997).
18. I. L. Medintz, H. T. Uyeda, E. R. Goldman, and H. Mattoussi, "Quantum dot bioconjugates for imaging, labelling and sensing," Nat. Mater. **4**(6), 435–446 (2005).
19. S. Coe, W.-K. Woo, M. Bawendi, and V. Bulović, "Electroluminescence from single monolayers of nanocrystals in molecular organic devices," Nature **420**(6917), 800–803 (2002).
20. B. Guzelturk, Y. Kelestemur, M. Z. Akgul, V. K. Sharma, and H. V. Demir, "Ultralow Threshold One-Photon- and Two-Photon-Pumped Optical Gain Media of Blue-Emitting Colloidal Quantum Dot Films," J. Phys. Chem. Lett. **5**(13), 2214–2218 (2014).
21. I. Robel, M. Kuno, and P. V. Kamat, "Size-dependent electron injection from excited CdSe quantum dots into TiO2 nanoparticles," J. Am. Chem. Soc. **129**(14), 4136–4137 (2007).
22. P. Reiss, J. Bleuse, and A. Pron, "Highly luminescent CdSe/ZnSe core/shell nanocrystals of low size dispersion," Nano Lett. **2**(7), 781–784 (2002).
23. Y. Shirasaki, G. J. Supran, M. G. Bawendi, and V. Bulovic, "Emergence of colloidal quantum-dot light-emitting technologies," Nat. Photonics **7**(1), 13–23 (2012).
24. H.-V. Han, C.-C. Lin, Y.-L. Tsai, H.-C. Chen, K.-J. Chen, Y.-L. Yeh, W.-Y. Lin, H.-C. Kuo, and P. Yu, "A Highly Efficient Hybrid GaAs Solar Cell Based on Colloidal-Quantum-Dot-Sensitization," Sci. Rep. **4**, 5734 (2014).
25. K. J. Chen, H. C. Chen, K. A. Tsai, C. C. Lin, H. H. Tsai, S. H. Chien, B. S. Cheng, Y. J. Hsu, M. H. Shih, C. H. Tsai, H.-H. Shih, and H.-C. Kuo, "Resonant-Enhanced Full-Color Emission of Quantum-Dot-Based Display Technology Using a Pulsed Spray Method," Adv. Funct. Mater. **22**(24), 5138–5143 (2012).
26. W. K. Bae, J. Kwak, J. Lim, D. Lee, M. K. Nam, K. Char, C. Lee, and S. Lee, "Multicolored Light-Emitting Diodes Based on All-Quantum-Dot Multilayer Films Using Layer-by-Layer Assembly Method," Nano Lett. **10**(7), 2368–2373 (2010).
27. J. Kwak, W. K. Bae, D. Lee, I. Park, J. Lim, M. Park, H. Cho, H. Woo, Y. Yoon, K. Char, S. Lee, and C. Lee, "Bright and Efficient Full-Color Colloidal Quantum Dot Light-Emitting Diodes Using an Inverted Device Structure," Nano Lett. **12**(5), 2362–2366 (2012).
28. B. S. Mashford, M. Stevenson, Z. Popovic, C. Hamilton, Z. Zhou, C. Breen, J. Steckel, V. Bulovic, M. Bawendi, S. Coe-Sullivan, and P. T. Kazlas, "High-efficiency quantum-dot light-emitting devices with enhanced charge injection," Nat. Photonics **7**(5), 407–412 (2013).
29. Y. Yang, Y. Zheng, W. Cao, A. Titov, J. Hyvonen, R. Manders Jesse, J. Xue, P. H. Holloway, and L. Qian, "High-efficiency light-emitting devices based on quantum dots with tailored nanostructures," Nat. Photonics **9**, 259–266 (2015).
30. L. Qian, Y. Zheng, J. Xue, and P. H. Holloway, "Stable and efficient quantum-dot light-emitting diodes based on solution-processed multilayer structures," Nat. Photonics **5**(9), 543–548 (2011).
31. J. Zhao, J. A. Bardecker, A. M. Munro, M. S. Liu, Y. Niu, I.-K. Ding, J. Luo, B. Chen, A. K.-Y. Jen, and D. S. Ginger, "Efficient CdSe/CdS quantum dot light-emitting diodes using a thermally polymerized hole transport layer," Nano Lett. **6**(3), 463–467 (2006).
32. V. Wood, M. J. Panzer, J. E. Halpert, J.-M. Caruge, M. G. Bawendi, and V. Bulović, "Selection of metal oxide charge transport layers for colloidal quantum dot LEDs," ACS Nano **3**(11), 3581–3586 (2009).
33. T.-H. Kim, K.-S. Cho, E. K. Lee, S. J. Lee, J. Chae, J. W. Kim, D. H. Kim, J.-Y. Kwon, G. Amaratunga, S. Y. Lee, B. L. Choi, Y. Kuk, J. M. Kim, and K. Kim, "Full-colour quantum dot displays fabricated by transfer printing," Nat. Photonics **5**(3), 176–182 (2011).

34. L. Kim, P. O. Anikeeva, S. A. Coe-Sullivan, J. S. Steckel, M. G. Bawendi, and V. Bulović, "Contact Printing of Quantum Dot Light-Emitting Devices," Nano Lett. **8**(12), 4513–4517 (2008).
35. H. M. Haverinen, R. A. Myllylä, and G. E. Jabbour, "Inkjet printing of light emitting quantum dots," Appl. Phys. Lett. **94**(7), 073108 (2009).
36. H. M. Haverinen, R. A. Myllyla, and G. E. Jabbour, "Inkjet Printed RGB Quantum Dot-Hybrid LED," J. Displ. Technol. **6**(3), 87–89 (2010).
37. M. Singh, H. M. Haverinen, P. Dhagat, and G. E. Jabbour, "Inkjet printing-process and its applications," Adv. Mater. **22**(6), 673–685 (2010).
38. W. Tang, L. Feng, C. Jiang, G. Yao, J. Zhao, Q. Cui, and X. Guo, "Controlling the surface wettability of the polymer dielectric for improved resolution of inkjet-printed electrodes and patterned channel regions in low-voltage solution-processed organic thin film transistors," J. Mater. Chem. C Mater. Opt. Electron. Devices **2**(28), 5553–5558 (2014).
39. S. Ma, L. Liu, V. Bromberg, and T. J. Singler, "Fabrication of highly electrically conducting fine patterns via substrate-independent inkjet printing of mussel-inspired organic nano-material," J. Mater. Chem. C Mater. Opt. Electron. Devices **2**(20), 3885–3889 (2014).
40. S. Günes, H. Neugebauer, and N. S. Sariciftci, "Conjugated polymer-based organic solar cells," Chem. Rev. **107**(4), 1324–1338 (2007).
41. C. N. Hoth, P. Schilinsky, S. A. Choulis, and C. J. Brabec, "Printing highly efficient organic solar cells," Nano Lett. **8**(9), 2806–2813 (2008).
42. T. Shimoda, K. Morii, S. Seki, and H. Kiguchi, "Inkjet printing of light-emitting polymer displays," MRS Bull. **28**(11), 821–827 (2003).
43. S.-C. Chang, J. Liu, J. Bharathan, Y. Yang, J. Onohara, and J. Kido, "Multicolor organic light-emitting diodes processed by hybrid inkjet printing," Adv. Mater. **11**(9), 734–737 (1999).
44. M. Wu, Z. Gong, A. J. Kuehne, A. L. Kanibolotsky, Y. J. Chen, I. F. Perepichka, A. R. Mackintosh, E. Gu, P. J. Skabara, R. A. Pethrick, and M. D. Dawson, "Hybrid GaN/organic microstructured light-emitting devices via ink-jet printing," Opt. Express **17**(19), 16436–16443 (2009).
45. J. G. Tait, E. Witkowska, M. Hirade, T.-H. Ke, P. E. Malinowski, S. Steudel, C. Adachi, and P. Heremans, "Uniform Aerosol Jet printed polymer lines with 30 μm width for 140 ppi resolution RGB organic light emitting diodes," Org. Electron. **22**, 40–43 (2015).
46. R. Aga, C. Jordan, R. S. Aga, C. M. Bartsch, and E. M. Heckman, "Metal Electrode Work Function Modification Using Aerosol Jet Printing," IEEE Electron Dev. Lett. **35**(11), 1124–1126 (2014).
47. R. Liu, H. Ding, J. Lin, F. Shen, Z. Cui, and T. Zhang, "Fabrication of platinum-decorated single-walled carbon nanotube based hydrogen sensors by aerosol jet printing," Nanotechnology **23**(50), 505301 (2012).
48. A. Mette, P. Richter, M. Hörteis, and S. Glunz, "Metal aerosol jet printing for solar cell metallization," Prog. Photovolt. Res. Appl. **15**(7), 621–627 (2007).
49. G. Cummins and M. P. Y. Desmulliez, "Inkjet printing of conductive materials: a review," Circuit World **38**(4), 193–213 (2012).
50. P. Chen, Y. Fu, R. Aminirad, C. Wang, J. Zhang, K. Wang, K. Galatsis, and C. Zhou, "Fully Printed Separated Carbon Nanotube Thin Film Transistor Circuits and Its Application in Organic Light Emitting Diode Control," Nano Lett. **11**(12), 5301–5308 (2011).
51. Y. T. Gizachew, L. Escoubas, J. J. Simon, M. Pasquinelli, J. Loiret, P. Y. Leguen, J. C. Jimeno, J. Martin, A. Apraiz, and J. P. Aguerre, "Towards ink-jet printed fine line front side metallization of crystalline silicon solar cells," Sol. Energy Mater. Sol. Cells **95**, S70–S82 (2011).
52. J. Wang, X. Cheng, M. Caironi, F. Gao, X. Yang, and N. C. Greenham, "Entirely solution-processed write-once-read-many-times memory devices and their operation mechanism," Org. Electron. **12**(7), 1271–1274 (2011).
53. T. Seifert, E. Sowade, F. Roscher, M. Wiemer, T. Gessner, and R. R. Baumann, "Additive Manufacturing Technologies Compared: Morphology of Deposits of Silver Ink Using Inkjet and Aerosol Jet Printing," Ind. Eng. Chem. Res. **54**(2), 769–779 (2015).
54. J. M. Hoey, A. Lutfurakhmanov, D. L. Schulz, and I. S. Akhatov, "A Review on Aerosol-Based Direct-Write and Its Applications for Microelectronics," J. Nanotechnol. **2012**, 22 (2012).
55. L. Chen, J. Xin, Z. Tianruo, and S. Goto, "Partial decoding scheme for H.264/AVC decoder," in *Intelligent Signal Processing and Communication Systems (ISPACS), 2010 International Symposium on*(2010), pp. 1–4.
56. K.-J. Chen, H.-C. Chen, M.-H. Shih, C.-H. Wang, M.-Y. Kuo, Y.-C. Yang, C.-C. Lin, and H.-C. Kuo, "The Influence of the thermal effect on CdSe/ZnS quantum dots in light-emitting diodes," J. Lightwave Technol. **30**(14), 2256–2261 (2012).
57. C. de Mello Donegá, M. Bode, and A. Meijerink, "Size- and temperature-dependence of exciton lifetimes in CdSe quantum dots," Phys. Rev. B **74**(8), 085320 (2006).

1. Introduction

In the past decade, the gallium nitride-based light-emitting diodes (LEDs) have been widely used as a solid-state lighting source or the backlight unit (BLU) of liquid crystal display (LCD) owing to their high luminous efficiency, low cost, long lifetime and environmental sustainability [1–6]. Nowadays, most of the power consumption in a LED panel can be

alleviated, but the passive components such as color filters can absorb a large portion of emitted photons [7,8]. In calculation, the light utilization efficiency (LUE) of the LCD display system is still lower than 2.8% [9], and this means the display needs to be operated at more than ten times of brightness in order to meet the expected output optical power. One solution is to incorporate individually addressable RGB light emitting devices which can replace the color filters. Two possible technologies are in competition now: organic LED and semiconductor-based LED. Organic LEDs can be fabricated in large area scale with reasonable cost, and they are compliant to different flexible substrates. However, the low brightness and short lifetime are limiting their wide development at present stage [10]. As for semiconductor based arrayed LEDs, they do not have such concerns [11–14]. But for a tri-color LED based technology, it is very difficult to grow three different active regions addressing different colors simultaneously on the same wafer, nor can we alter the color once the epitaxial growth is finished. If the material growth is split into multiple steps, the yield and the expenses are expected to be undermined. To overcome this problem, colloidal quantum dots (CQDs) can be a great choice. The CQDs are usually synthesized by chemical solution process [15–17]. and possess unique properties such as high quantum yield [18–20], size-dependent emission wavelength [21,22], and narrow emission linewidth [23,24], etc.. In our technology, the color rendering can be optimized by properly selecting the QDs and the growth effort can be focused onto the UV LED. In addition to these great benefits, compared to our previous study [25], the aerosol jet represents a great step forward on the resolution improvement. The previously demonstrated pulsed-spray technology is good for large-scale device (in millimeter) and more suitable for white light generation in our opinion. The current AJ method can shrink the pixel size to 35 μm in this study and even to 10 μm in theory. Combining with micro-array LEDs, a vivid full color and high resolution display is possible. In the previous studies, many researchers demonstrated electrically-driven CQD-based LEDs with very good lighting characteristics. In the past, the CQDs emitters were used as the active layer and manufactured an organic–inorganic hybrid device structure to have the electroluminescent characteristics [26–30]. However these devices usually suffered from the weak luminous efficiency (below 20 lm/w), limited choices for carrier transport matching layers, and shorter-than-expect emission lifetime. To relieve from these limitation, we believe using CQD layer as a passive photon conversion mechanism should suffice for high quality and multiple color generation. Without the need to line up the energy bands for carrier transportation, we can put more efforts on optimizing the color quality and efficiency of the devices. In this study, a luminous efficiency as high as 32 lm/W can be demonstrated.

If CQDs are chosen for RGB pixels, the deposition method needs to be thoroughly investigated. In order to spraying the QDs uniformly, different methods have been used to deposit the QDs for display technology and light emitting applications, including spin coating, mist coating, pulse-spray coating, stamp printing, and inkjet printing [25,31–36]. Among these manufacturing technologies, spin coating, mist coating, and pulse-spray coating are for the low-resolution patterns and bear high material loss [25,35]. For the stamp printing, it can achieve multi-color pixel arrays but it is difficult to alignment accurately for various color pixels. Moreover, the inkjet printing is a deposition technique for large-area application with high-resolution patterning and low material waste [37]. In the last years, inkjet printing is a well-known technology in the field of printed electronics and it has potential in other applications such as transistors, antennas, solar cells, sensors, and LEDs [38–44]. Aerosol jet printing, on the other hand, also allows the precise, mask-less, and non-contact deposition of liquids containing functional materials. Many published results have applied this technology to obtain great progress in light emitting diodes, metal electrode writing and printed circuitry for gas sensors [45–48]. However, in comparison to inkjet printing, this technology is relatively young and has the potential to provide higher resolution.

The aerosol jet printing is a direct-writing and non-contact deposition technology. A very similar method named ink jet printing has been in the commercial applications for almost 30

years [49]. The ink jet printing is a more mature technology compared to aerosol jet printing [50–52], but aerosol jet printing has several advantages such as a higher resolution, less strict requirements for the viscosity of ink, and a bigger working distance [53,54]. The resolution of aerosol jet printing can achieve less than 30 μm, while the typical resolution of ink jet printing is 50 μm. Moreover, the ink viscosity of aerosol jet printing is in the range from 0.5 to 2000 cP, but the ink jet printing only can suit for low viscosity solutions (<20 cP). Therefore, the aerosol jet printing is more suitable for the deposition of QDs in our experiments.

In this paper, we report a BLU-free full-color LED based display by combining UV micro LED arrays with RGB QDs via aerosol jet printing. Furthermore, in order to increasing RGB emission intensity and fully utilize the UV light, a DBR with a stopband centered at 400 nm was used in the LED arrays. Therefore, combining the micro LED arrays and RGB QDs with highly reflective DBR exhibits a full-colored display technology and provides an alternative method for display applications.

2. Experiments

The UV-visible absorption and photoluminescence (PL) spectroscopy were characterized for the three different types of QDs. These RGB QDs were purchased from the UT-dots Corporation for our experiment, and they are in core-shell type structure with chemical ligands on the outer shells. The quantum yield, according to vendor's data, is higher than 50%. Composed of CdSe or CdS, their crystal structures are hexagonal Wurtzite structure. As shown in Figs. 1(a), 1(c) and 1(e), the absorption and emission spectra for the CdS and CdSe/ZnS core-shell QDs are plotted, and the onset of the absorption or peak of emission is controlled by the quantum confinement effect (the size of the QDs).The PL spectra of the three types of QD in toluene were measured using a 365 nm excitation, and showed different peaks at 450 nm, 520 nm, and 630 nm, respectively. Regarding the chemical composition of the QDs, CdS was used for emission wavelengths shorter than 450 nm, and CdSe/ZnS core-shell was used for emission wavelengths longer than 520 nm. The absorption spectrum of different types of QDs shows the QDs can absorb the higher energy photons than the emission wavelength. Figs. 1(b), 1(d) and 1(f) show the images of the colloidal QDs in toluene under 365 nm UV light excitation.
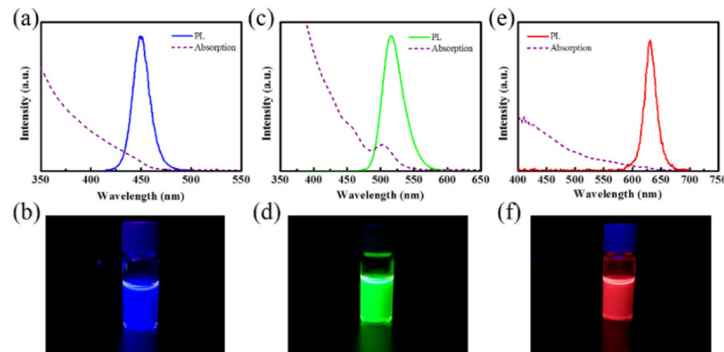

Fig. 1. UV-visible absorption and PL emission spectra of QDs with the emission colors of (a) blue, (c) green and (e) red. (b) blue, (d) green and (f) red are the photos of quantum dot solution under UV excitation.

Further structural characterizations were performed using a transmission electron microscope (TEM) and high-resolution TEM (HRTEM). Figs. 2(a), 2(c) and 2(e) show the transmission electron microscopy (TEM) image of the QDs with 450 nm, 520 nm, and 630 nm emission peak. The inset charts show the corresponding selected-area electron diffraction (SAED) patterns of the three QD samples. These QD samples were considerably uniform in morphology and exhibited a narrow size distribution. Moreover, the emission peak of QDs

could be tunable based on the particle diameters. When the QD particles were larger in size, the emission peak wavelength was redshifted. The average diameter of blue, green, and red QD samples was measured as 2.47 ± 0.46 nm, 6.17 ± 1.23 nm, and 9.29 ± 0.95 nm, respectively. The line width of PL for blue, green, and red QDs was 20 nm, 36 nm, and 23 nm, respectively. Because green QDs have a relatively wide size distribution of 19%, they exhibited a broader PL line-shape than blue and red QDs. Figs. 2(b), 2(d) and 2(f) show the detailed crystallographic structures of the three QD samples, and the lattice planes can be observed clearly.

Fig. 2. Typical TEM images of QDs with the emission colors of (a) blue, (c) green, and (e) red. The corresponding HRTEM images are shown in (b), (d), and (f), respectively.

When considering for the possible choices of the excitation source, there are two reasons for us to choose UV LED instead of blue one: excitation efficiency and color mixing. Even though it is much easier to have a blue LED as the pumping source to remove the need for blue QD and save the cost of LEDs, the combination of the UV LED and RGB QDs should be much better than the blue LED and GB QDs. The absorption profiles from QDs clearly demonstrate higher efficiency in the UV band than the blue band. So if we use UV as the pumping photon, all three QDs can be fully excited. If blue photons are used as the excitation sources, they are less efficient to pump green QDs and thus more green materials are needed in the device which might offset the cost-saving brought by using blue LEDs. The second problem of using blue LED is that the color mixing is difficult due to strong blue spectrum in the overall device output. As we could observed from the current UV layout in our experimental results, the UV peak is still very dominant after the QD absorption. While UV photons are not counted for the color mixing, the blue photons do. If we replace the UV LED with blue one, the output of our device will be strongly affected by blue peak and the CCT or CRI will be very poor. So for the purpose of color quality, the UV LED is a better candidate to have a more evenly distributed RGB output spectrum. As shown in Fig. 3, standard multiple quantum well (MQW) LED were grown on sapphire substrates for the micro LED arrays. The UV passive-matrix micro-LED arrays were fabricated on UV epi-wafers with peak wavelength 395 nm, respectively. The chip size was 5 x 5 mm^2 with a display area of 4.48 x 4.48 mm^2, consisting of 128 x 128 arrays of 35 μm micro-emitters with a center-to-center pitch of 40 μm. LED pixels of the micro-LED array in the same column share a common electrode of the n-type GaN. Thus it is necessary to isolate all the stripes of micro-LED array. This is realized by creating isolation trenches via dry etching of GaN down to the

sapphire substrate. Silicon dioxide (SiO$_2$) was used as hard mask for dry etching. The p-electrode stripes were defined on top of the transparent resist and connected to all the pixels in the same row. When the micro LED array was finished shown in Fig. 3(a), we use the aerosol jet printing method to spray the RGB QDs on the micro LED array sequentially. In the aerosol jet printing method, the QDs solution is aerosolized and entrained in a gas stream. There are two options for generating the aerosol: pneumatic and ultrasonic. The aerosol stream is directed to a print head where it is aerodynamically focused by a coaxial sheath gas flow. The concentrations of the RGB QDs are approximately 5 mg/mL. We adjusted the aerosol jet printing process parameters, including working distance, stage speed, carrier gas flow rate, sheath gas flow rate, and atomization frequency, to obtain the spraying linewidth of 35μm. The ratio of carrier gas flow rate and sheath gas flow rate is the most important parameter in the adjustment for opportune spraying linewidth. During the QD spray, the system parameters need to be optimized. The working distance and stage speed between the nozzle and the substrate, which are 1mm and 10mm/s respectively, are fixed in our cases and only carrier gas flow rate and sheath gas flow rate are two changeable parameters. Although the concentrations of the RGB QDs are about the same, the different particle sizes will alter the deposition result such that different flow rates are needed. Usually we need to increase the carrier gas flow rate as the particle size grows. At the same time, when the carrier gas increases, the flow rate of sheath gas needs to be increased as well to hold the linewidth of the deposited QDs. Then, the RGB QDs were sprayed onto the surface of the micro LED array using the aerosol jet method in the sequence of red, green, and blue, as shown in Figs. 3(b)-3(d). The operation of spray was precisely controlled by a computer system, and the quantity of the QDs can be monitored instantaneously. Finally, in Fig. 3(e), a distributed Bragg reflector (DBR) was capped on the top of micro LED arrays in order to reducing the leaked UV light for display applications. Thank you for your kindly advices. The resolution of our current display is 282 pixels per inch (PPI) in full color. The Retina Display of Apple Inc., which equipped with 960 X 640 resolution in a 3.5-inch screen, is equivalent to 326 ppi and based on TFT technology [55]. Figure 4 shows the photo image and schematic pictures of aerosol jet printing in this experiment.
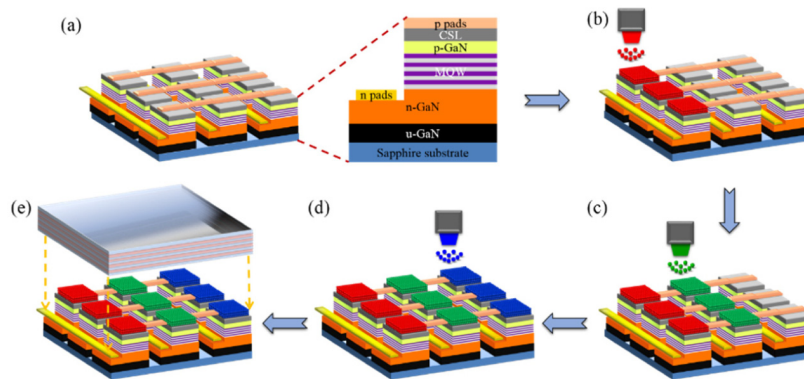

Fig. 3. The process flow of the full-color emission of quantum-dot-based micro LED display.
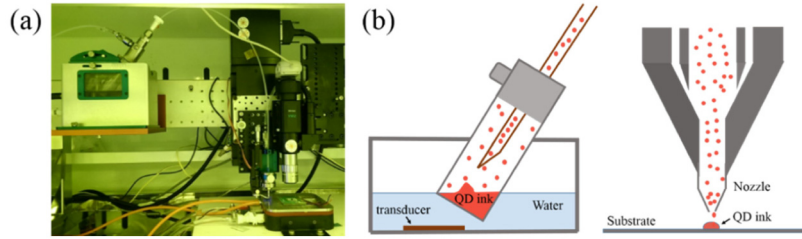
Fig. 4. (a) The image of aerosol jet printing. (b) The schematic pictures of aerosol jet printing.

As for the deposited QD profile, our QD layer is slightly different from other people's or our previous study. The main reason is because our deposition of QD is on the top of the UV LED mesa, as can be seen in Fig. 5(a). To minimize the size of the QD deposit, a bell-shape profile is necessary, and adjustment on the thickness for individual color is also critical to keep the strength of each color's emission the same. We measured the 3D surface profile of the deposited RGB QDs on the micro LED arrays, by the laser scanner microscope as shown in Fig. 5(b). From the cross section profile of laser scanner microscope image, the average height of red, green and blue QDs are 2.879 μm, 5.581 μm and 6.462 μm, respectively. The height of the same color QD lines are almost the same and the height standard deviation is less than 0.16 μm. So we could conclude that the coating is quite uniform within the same process run among different colors. However, we have to point out that due to the higher priority to the optimization of the light output, the coating thickness were different from run to run and the uniformity is thus not investigated at present.
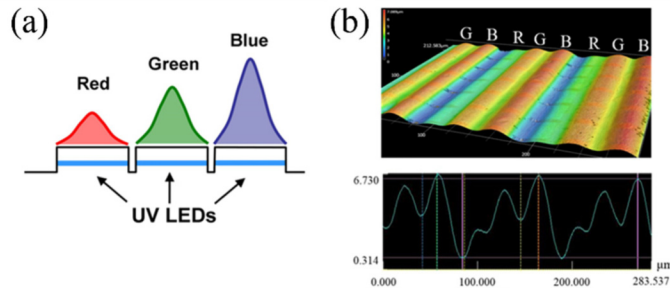

Fig. 5. (a) The deposition profiles for our RGB QDs on the UV LED, (b) The surface profile image of jet-printed QDs scanned by the laser microscopy.

3. Results and discussion

Figure 6. shows the fluorescence microscopy image of sprayed the RGB QDs micro LED array, and the excitation wavelength of the fluorescence microscopy is 365 nm. The size of the pixel is 35 μm × 35 μm and the pitch between the pixels is 40 μm. There are 128 columns of RGB lines and the line width was controlled at 35 μm, which can just cover one pixel, as shown in upper right chart of Fig. 6. The upper left of Fig. 6 shows the full-size sample under UV excitation.
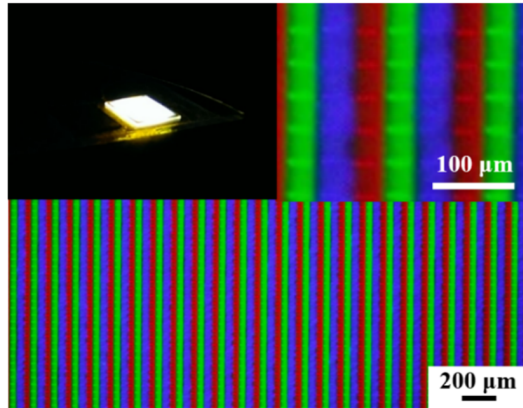
Fig. 6. The photo image of sprayed QDs micro LED array under the fluorescence microscopy.

The micro-LED array emits the photons of 395 nm which can excite the RGB QDs deposited on the surface of the individual LED. However, due to the thin thickness of the QD layer, the UV photons from the underneath LED cannot be absorbed completely. If this type of device is going to be used for display or lighting applications, extra care needs to be taken to these leaked UV rays. The best way to deal with this situation is to lay down a layer of DBR to increase the recycling of the UV photons. In our design, a 17.5-pair HfO_2/SiO_2 multiple-layer structure was integrated into the micro-LED array. As shown in Fig. 7(a), this DBR provides 90% of reflectance at 395 nm and high transmission (around 90%) at 450 nm (Blue), 520 nm (Green) and 630 nm (Red) bands.

Figure 7(b) shows the relative PL intensity of the passive-matrix micro LED array sample with DBR under 325 nm pumping source, compared with the reference without DBR. The result demonstrates that the UV micro LED array sample with DBR have higher intensity in blue, green, and red components than the reference without DBR. The laser spot size of PL system we used was about 70 μm, so it is difficult to cover RGB QD entirely, and this causes the uneven intensity in the measurement.
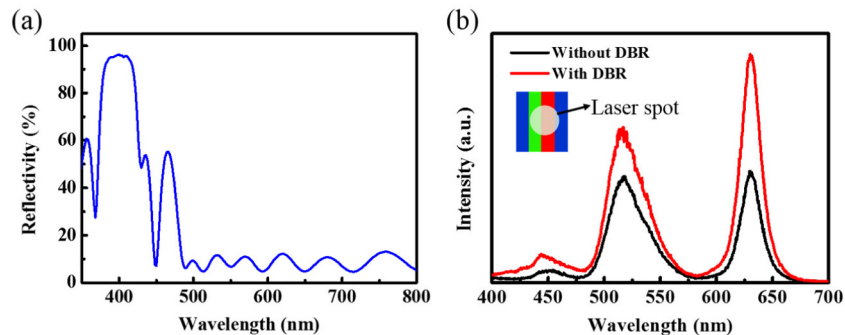

Fig. 7. (a)Measured reflectance spectrum of 17.5-pair HfO_2/SiO_2 distributed Bragg reflector (DBR). (b)The relative PL intensity of the sprayed QDs samples with and without DBR.

Similar enhancement can be observed in the electroluminescence (EL) spectra, as shown in Fig. 8(a). The driving current of each LED is 20 mA and the spectra with and without DBR were taken. From the measurement, a pronounced UV peak (at 395 nm) is an indicator of less-efficient pumping, while the red, green, and blue signals are not strong. After DBR is added, the strong reflection at UV band successfully suppressed the 395 nm peak and increase the visible intensities by 194% (blue), 173% (green) and 183% (red). Figure 8(b) demonstrate the micro-LED array with QDs in full operation. The electrical layout of this array enables

individual addressable excitation of each pixel. Figure 9 shows the large scale monochromatic light emission from the QD micro LED arrays.
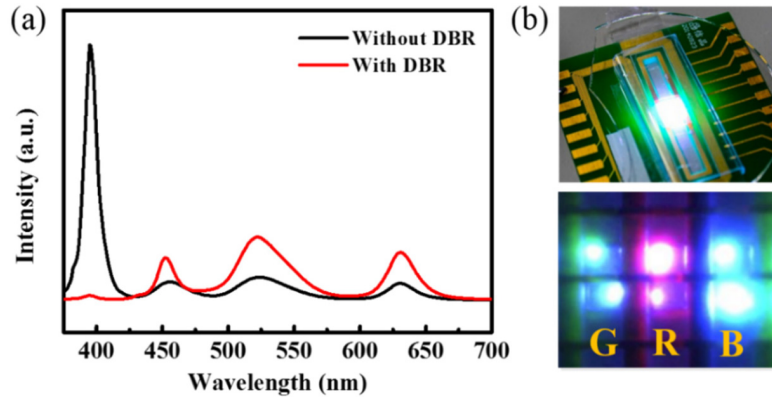

Fig. 8. (a) The emission spectra with and without the DBR structure. (b) Top: the sprayed RBG QDs micro LED display device in action; bottom: representative image of RGB pixels.
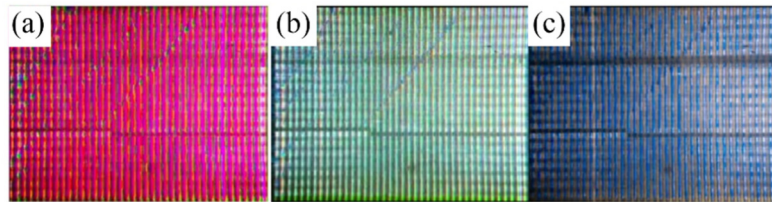

Fig. 9. (a)-(c) The large area monochromatic light emission (red, green, and blue) of the QD micro LED arrays.

Additionally, the color coordinates of three QDs were measured by a spectrometer and plotted on the CIE 1976 chromaticity diagram as shown in Fig. 10. The CIE coordinates of the QDs related emissions were compared to the National Television System Committee (NTSC) standard color triangle. The saturated color provided by narrow-linewidth emission of QDs ensure the maximum coverage on the CIE diagram. The area inside the yellow dash triangle shows the maximum color gamut that can be projected by the RGB QDs, which is 1.52 times of the NTSC color gamut (dash-dot line). When the color of the QDs are changed, so does the triangle in the plot.
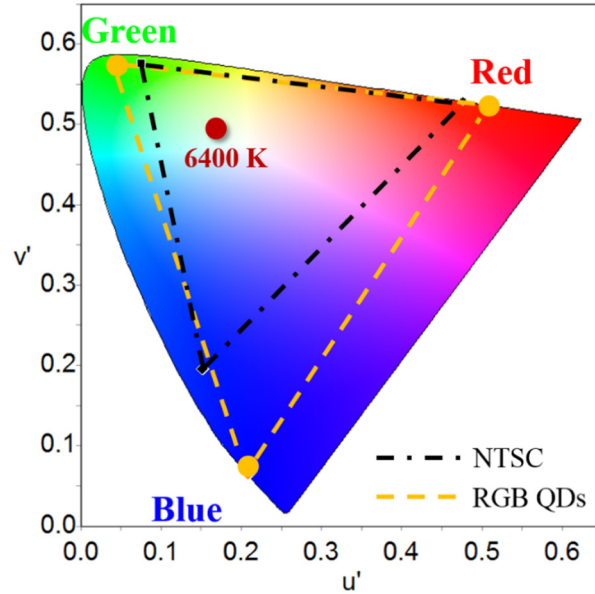
Fig. 10. The CIE1976 color space chromaticity diagram of the QD display technology and NTSC.

Figure 11(a) shows the normalized electroluminescence (EL) spectra of the UV micro LED array with RGB QDs and DBR structure from 100 mA to 1 A of total input current. There is certain discrepancy between Fig. 8(a) and Fig. 11(a) spectra, and the root cause behind this is the degradation of the QD material. Figure 8(a) was taken right after the QD sprayed onto the UV LED while the data in Fig. 11 were tested after several days. In our experience, the emission intensity of our QD layer can decay rapidly in the first 24 hours, and keep stable for a long time. So when the absorption and the emission capability of the QD layer became weaker, the portion of UV photon pass through the device became higher and the visible photons became fewer. So it is very important to improvement the QD lifetime in the air to have an efficiency QD light source. The CIE1976 coordinates at various driving currents are shown in Fig. 11(b). In our test, the $\Delta u'v'$ is 0.0191 from different driving currents of 100 mA to 1 A. The increments of each color under increased injection currents are not uniform. While it is understandable that this increment of intensity is larger at low current and smaller at high current due thermal issue, it is also important to notice that the red QD is gaining at high current as blue and green stop growing after 700 mA. This phenomenon results in the movement of bias-dependent correlated color temperature (CCT) forwards lower value as we increase our input. Figure 11(d) shows the result of the luminous efficacy of radiation (LER) of our structure. The LER was calculated using the following formula:

$$\text{LER} = 683 \frac{lm}{W} \frac{\int V(\lambda)P_{white}(\lambda)\,d\lambda}{\int P_{white}(\lambda)\,d\lambda}. \tag{1}$$

where 683 lm/W is a normalization factor, $V(\lambda)$ is the human eye sensitivity function, and $P_{white}(\lambda)$ is the spectral power density of the light source.

Figure 11(c) shows the current-dependent CCT, which spread between 6408 K and 5460 K. This variation is probably caused by the different thermal performances of QDs with different emission wavelengths [56]. The exciton lifetimes of smaller dots can decrease dramatically when the device temperature rises [57]. In our case, as input current increases,

the module temperature rises accordingly. So we will expect larger drop in blue QD intensity, and thus the CCT becomes lower.

The long-term stability of such devices is also an important issue for commercial success. Due to the small scale of the individual device, the evaluation of the lifetime is more plausible to perform in the standard LED package. The existing data based on the on-shelf storage aging test showed a rapid drop in the first 24 hours. After that, stable output (but with about 20% of the original value) can be expected from the QD material.
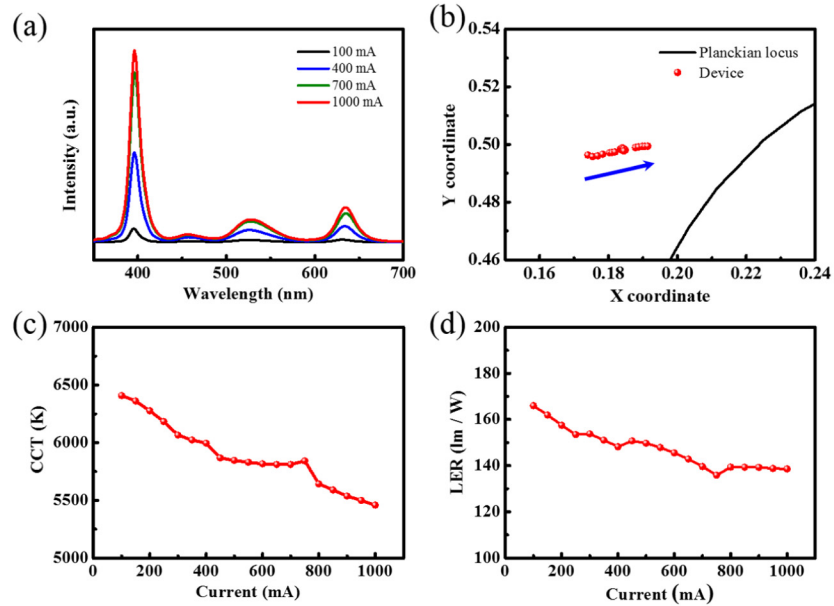

Fig. 11. (a) The relative emission spectrum of the micro LED array with RGB QDs and DBR structure under various drive currents (from 100 mA to 1 A, from bottom to top curves). (b) The zoom-in traces of CIE1976 chromaticity diagram of our structure under different driving current. (c) The CCT and (d) the luminous efficacy of optical radiation of UV micro LED array with RGB QDs and DBR structure under currents between 100 mA and 1 A.

4. Conclusion

In conclusion, we demonstrate a micro-sized LED array with independently addressable RGB pixels by applying AJ technology with colloidal quantum dots. The initial results show promising white light generation and good LER under various injection currents. This study investigates a high-resolution pixelated array which can be used for display technology. We believe this technology shall be disruptive for future generation of light-emitting devices.

Acknowledgment